To be published in Journal of the Optical Society of America B:

Title: Impact of Pump Beam Spot Size on Semiconductor Carrier Dynamics in Optical-Pump-THz-Probe Spectroscopy

Authors: Yannic Staechelin,Tobias Kroh,Franz Kaertner,Holger Lange

Accepted: 23 June 23

Posted 28 June 23

DOI: https://doi.org/10.1364/JOSAB.496228

Impact of Pump Beam Spot Size on Semiconductor Carrier Dynamics in Optical-Pump-THz-Probe Spectroscopy

YANNIC U. STAECHELIN[1,*], TOBIAS KROH[2,3], FRANZ X. KÄRTNER[2,3], HOLGER LANGE[3,4]

[1] *Institute of Physical Chemistry, Universität Hamburg, Martin-Luther-King-Platz 6, 20146 Hamburg, Germany*
[2] *Center for Free-Electron Laser Science CFEL, Deutsches Elektronen-Synchrotron DESY, Germany*
[3] *The Hamburg Centre for Ultrafast Imaging, Luruper Chaussee 149, 22761 Hamburg, Germany*
[4] *University of Potsdam, Institute of Physics and Astronomy, Karl-Liebknecht-Straße 24, Potsdam, Germany*
[*] *yannic.staechelin@uni-hamburg.de*

Abstract: Optical-Pump-Terahertz-Probe experiments (OPTP) are widely employed to study the dynamics of photoexcited carriers in semiconductors. In these experiments, due to the long wavelength nature of the Terahertz (THz) probe radiation, the probe beam can only be focused to a spot size in the mm range. To ensure homogeneous excitation of the probed sample region, a significantly larger optical pump beam spot size must be used, which is often difficult to implement in the experiment. Frequently used experimental geometries employ beam paths which result in small pump beam spot sizes, leading to spectral distortions of the sample response, translating to uncertainties in calculated THz conductivities and fitted Drude conductivity models, for example. We investigate the influence of the pump beam spot size on benchmark OPTP experiments and evaluate model calculations to estimate the induced deviations. We demonstrate the impact of this effect on the acquired data with different dependencies on the investigated sample and the employed experimental configuration. We can provide guidelines for optimal configurations for the most commonly employed experiments.

1. Introduction

Optical-Pump-THz-Probe spectroscopy (OPTP) is a powerful technique to study the electrical properties of photoexcited semiconductors. As a non-contact technique, it is especially useful for nanomaterials, which are inherently difficult to make electrical contact to [1–4]. In OPTP, a femtosecond optical laser pulse is used to photoexcite the sample of interest. After a variable delay time τ, a THz pulse probes the photoinduced changes in THz transmittance of the sample. The measurement of the differential THz transmittance of excited and unexcited sample leads to the photoconductivity in the THz frequency range. Experimentally, the THz probe pulse is commonly generated by optical rectification and spans a frequency range from 0.1 to 2 THz, which corresponds to wavelengths of about 3 to 0.15 mm [5–7]. Off-axis parabolic mirrors (OAPs) are used to collimate and focus the THz radiation onto the sample. As the relative bandwidth of the THz probe pulse is very large, higher frequencies (i.e. shorter wavelenghts) are focused more tightly than lower frequencies (i.e. longer wavelengths). In most cases, the optical pump beam is transmitted through a hole in the focusing OAP for collinear beam propagation (cf. Figure 1(a)). The size of the hole is typically in the milimeter range and limits the spot size of the optical pump beam. Large holes would lead to distortions in the THz beam profile as well as loss of THz intensity. Comparably small pump beam spot sizes result in the lower THz probe frequencies, which have a larger spot size, propagating through relatively less excited parts of the sample than the higher THz frequencies, that are focused to smaller spot sizes. This leads to an attenuation of the measured differential THz-electric field at low THz frequencies, effectively shifting the differential THz spectrum to higher frequencies. When evaluating the

differential data, for example for calculating the complex photoconductivity and fitting e.g. a Drude conductivity model, the frequency-dependence has to be weighted accordingly.
Beard *et al.* demonstrated the problem experimentally in OPTP measurements on GaAs. They concluded that for a homogeneous excitation, the pump beam spot size should be at least two times larger than the probe beam spot size [8]. Dakovski *et al.* modelled the pump-beam-spot-size-dependent THz response as radiation from a pump-induced current driven by the THz electric field and suggested the use of metallic apertures for the THz radiation to reduce the probed area of the sample [9]. Strait *et al.* defined an overlap factor to account for the mismatch in pump and THz spot sizes and correct the differential spectra [10].
Depending on the discussed quantities and varied parameters, the uncertainties resulting from insufficient overlap might not be too problematic. For example, discussing differences in the high-frequency part of the complex conductivity could be robust. In similar ways, time-constants of photoinduced changes or excitation-power dependencies might be unperturbed by spot-size problems as they might lack significant frequency dependencies. In the present work, we try to deliver a comprehensive picture of how spot size-related problems occur in the most common OPTP experiments on semiconductors. We investigate how they reflect in typically discussed data and which part of the data can be regarded as unproblematic. For this purpose, we performed OPTP with a setup geometry found often across the literature. We investigated two reference semiconductor materials, silicon and CdS nanostructures and we show where focus-related errors occur. We model the problem using plain, accessible calculations in order to explain how errors evolve and under which experimental conditions reliable data can be recorded. We consider the influence of the investigated sample as well as the experimental setup, aimed to serve as primer for carefully designing experiments.

2. Experimental setup

For our pump-beam-spot-size study, we employed the most widely used OPTP setup geometry (Fig. 1(a)) [5, 6]. An amplified Ti-sapphire laser system (Spitfire-Ace, 800 nm, 1 kHz, 35 fs; Spectra Physics) was employed as excitation source. The laser beam was split into three arms for the optical pump beam, the THz generation and the THz detection beam. For the optical pump beam, the 800 nm laser fundamental was frequency-doubled to obtain 400 nm using a BBO crystal. The THz radiation was generated in a ZnTe crystal by optical rectification. A weak part of the 800 nm fundamental was retained for electro-optical sampling (EOS) of the THz electric field in another ZnTe crystal. Fig. 1(b) shows the THz probe spectrum as measured with THz time domain spectroscopy (TDS). OPTP spectra of the two reference materials (CdS nanowires and Si) were measured with three different optical pump beam spot sizes (0.54 mm, 1.16 mm and 3.02 mm beam radius). To assess size-dependencies, the pump-beam-spot sizes were set by using different lenses to focus the optical pump beam onto the samples. For the collinear pump-probe geometry, the focus points were placed inside the through-hole of the OAP so that the beam diverged before impinging onto the sample. Since the diameter of the through-hole in the OAP (1.5 mm diameter at the OAPs front surface and 5 mm diameter at its backside) sets an upper limit to the pump beam spot size, we switched to a non-collinear pump-probe geometry for experiments with the largest pump beam spot size. There, the pump hits the sample at an angle, which leads to a distortion of the spherical pump beam profile into an elliptical profile and adds a temporal delay between opposite sides of the pump beam. The pump beam radii ($1/e^2$ intensity) were measured by knife-edge scans. In the measurements under non-collinear geometry, the elliptical beam profile impinging onto the sample was calculated using the known angle of incidence. We treated the elliptical beam profile as an effective spherical beam of the same area. Beam radii of collinearly propagating pump beams were 0.54 mm and 1.16 mm. The effective beam radius of the non-collinear pump beam was 3.02 mm, which corresponds to an ellipse with radii of 2.71 mm and 3.36 mm. The pump fluence was ensured to be the same in

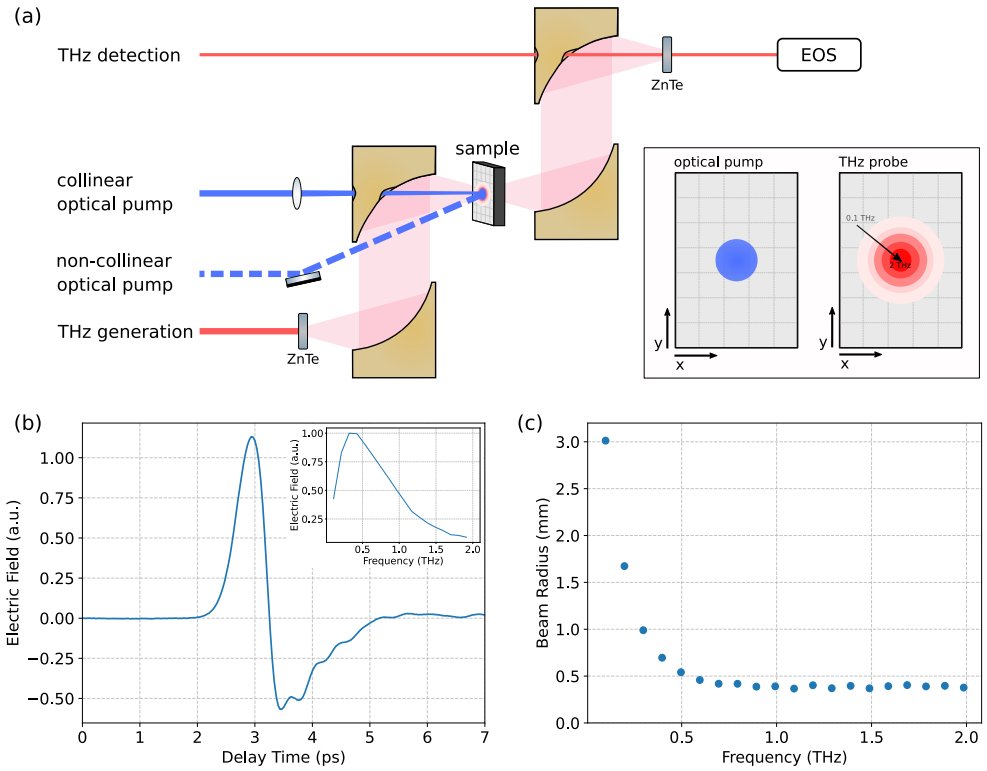

Fig. 1. (a) Experimental setup of the Optical-Pump-THz-Probe experiment and schematic representation of the spot-size problem: The optical pump beam spot size is typically smaller than the THz probe beam spot size to measure undistorted OPTP data. However, the probe beam can only be focused to a certain spot size due to its long wavelength nature. Additionally, the THz frequencies in the probe beam spot are inhomogenously distributed (frequency-dependent focus). (b) THz-electric field of the probe beam as measured by THz-TDS. The corresponding spectrum is diplayed as inset. (c) Frequency-dependent beam radii ($1/e^2$) of the THz probe beam as measured using the knife-edge technique at the sample position.

all experiments and set to 60 µJ/cm^2. The spatial distribution of the different frequencies of the THz probe pulses at the focus spot was obtained by combining the knife-edge technique with THz-TDS. By recording spectra vs the insertion of the blade into the focused beam, the THz radii of each frequency component were obtained (Fig. 1(c)). As expected, we find that longer wavelengths are focused to larger spot sizes. The beam radii do not perfectly follow the expected $1/\lambda$ behavior for high THz frequencies. For the focusing conditions in our experiment, all frequencies above 1 THz are focused to the same spot size. The knife-edge data is shown in more detail in Figure S1.

3. Discussion

3.1. Spectral distortions in the differential THz field

Fig. 2(a) shows the photoinduced changes in the THz waveform transmitted through a Si wafer after excitation with different pump beam spot sizes. Fourier-transformation of this data yields the differential THz spectra, shown in Fig. 2(b). As expected, we observe a shift towards higher

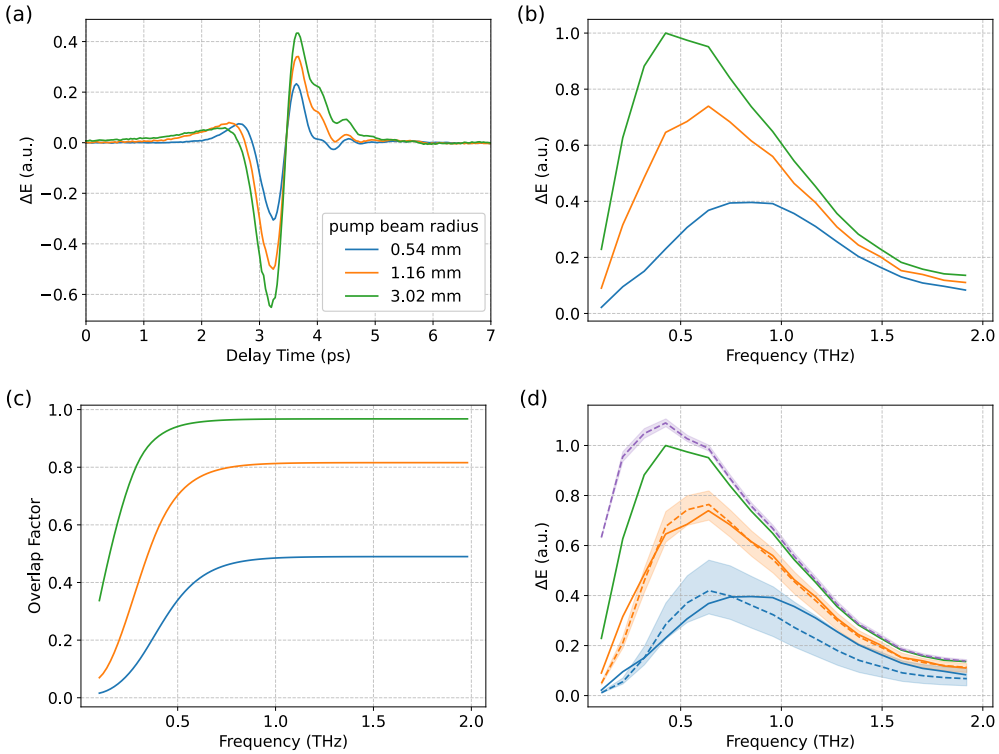

Fig. 2. (a) Photoinduced changes in the THz waveform ΔE transmitted through a 1" Si Wafer 30 ps after excitation with λ = 400 nm and three different pump beam spot sizes. (b), (c) and (d) use the same colour code. (b) Fourier-transform of the data shown in (a). For larger pump beam spot sizes, higher differential fields are measured at equal excitation fluences. Also, a shift towards lower frequencies is observed. (c) Frequency-dependent pump-probe beam spot overlap factor for the three different pump beam spot sizes. (d) The solid lines show the same data as in (b) and the dashed lines show simulated differential fields. The shaded areas present the uncertainty due to the errors in the characterization of the pump and probe beam radii. Using the overlap factors plotted in (c), the purple dashed line shows the differential electric field for an infinite large pump beam spot size, calculated from the data measured with a pump beam radius of 3.02 mm. From this, we can calculate the differential electric field for the pump beam spot sizes of 0.54 mm and 1.16 mm (dashed orange and green lines).

THz frequencies when employing smaller pump beam spot sizes. We define an overlap factor that scales with the carrier density within the sample material through which the THz radiation propagates. A value of 0 means that the THz radiation traverses an unexcited region of the sample, whereas a value of 1 means that the THz radiation traverses the sample area subject to maximum excitation given the specific excitation conditions employed. This plain model calculation allows analyzing the distortions in the differential THz spectra depending on the pump beam spot size for thin films or thin photoexcited layers. In the first step, the spatial charge carrier distribution in the sample after excitation is modelled, assuming an excitation density, at which the spatial charge carrier density is proportional to the excitation beam intensity, i.e. no non-linear effects. In the second step, the spatial THz electric field distribution is calculated for every frequency component of the THz pulse, using the frequency-dependent THz beam spot sizes shown in Figure 1(c). Both the spatial charge carrier distribution as well as the spatial THz

electric field distribution are modelled as two-dimensional Gaussians. Since in less excited parts of the samples there will be less interaction of the THz probe pulse with photoexcited charge carriers, the THz electric field profiles are now weighted with the charge carrier distribution profile; again assuming interaction in the linear regime. Integration of the THz electric fields over the entire sample area yields an effective THz spectrum that can be compared with the initial THz spectrum to calculate a frequency-dependent pump-probe overlap factor OF. The overlap factor is described by

$$OF(\nu) = \frac{1}{2}\left(\frac{w_{pump}^2}{w_0(\nu)^2 + \frac{1}{2}w_{pump}^2}\right), \tag{1}$$

where ν is the THz frequency, w_{pump} is the pump beam spot size and $w_0(\nu)$ is the frequency-dependent THz probe beam spot size (the derivation for this expression is provided in the SI). Figure 2(c) shows this overlap factor for the three pump beam spot sizes employed in this work. As expected, the overlap factor is higher for larger pump beam spot sizes. Also, at low THz frequencies, i.e. long wavelengths, the overlap factor drops significantly. The smaller the pump beam, the higher the THz frequency at which this drop occurs. This means, the spectral distortion in the measured differential THz E-field increases. Using the overlap factors from Figure 2(c), we can calculate the actual differential THz spectrum that would be measured with infinitely large pump spot size from the measured differential THz spectra. For this calculation, we use the spectrum obtained with the largest pump spot and, therefore, best SNR. The dashed purple line in Fig. 2(d) shows this undistorted differential THz spectrum. From there, we can calculate the differential THz spectra at the two smaller pump beam spot sizes and find good agreement with the measured data, validating our overlap factors. Similar experiments were performed on CdS nanowires and show the same trends (cf. Fig. S2). Our results show that for our THz focusing conditions, for THz frequencies larger than 1 THz, the differential THz electric field is not distorted spectrally even with pump beam spot sizes as small as 0.54 mm.

3.2. Influence on estimated conductivities

From the measured differential THz spectra, the complex photoconductivities of thin photoexcited films are commonly calculated employing the Tinkham-Glover formula [2]

$$\sigma(\omega) = -\epsilon_0 c(1 + n_{\text{substrate}})\frac{\Delta T(\omega)}{T(\omega)}, \tag{2}$$

where ϵ_0 is the vacuum permittivity, c is the speed of light and $n_{\text{substrate}}$ is the refractive index of the substrate and $\Delta T(\omega)$ and $T(\omega)$ are the Fourier-transform of the differential THz waveform after photoexcitation and the THz waveform transmitted through the unexcited sample, respectively. Thus, the distortion in the measured differential THz spectrum linearly transforms on to the calculated complex photoconductivities. Fig. 3 exemplarily shows simulated distortions in the real and imaginary photoconductivity of a sample exhibiting (a) Drude response and (b) Lorentz-Drude response when pumped with a beam radius of 1.16 mm and probed with the THz focusing conditions that we found in our setup. Especially when aiming at discussing the dc limit, discrepancies can be strong.

3.3. Influence on dynamics

3.3.1. Temporal evolution of photoconductivity

The main advantage of OPTP is the possibility to study the temporal evolution of the real and imaginary photoconductivity with the pump-probe delay time [4, 11, 12]. There, measuring the differential electric field at the THz delay of the peak electric field of the undisturbed THz pulse yields approximately the frequency averaged real photoconductivity, whereas the same measurement at the THz delay of the zero-crossing of the undisturbed THz pulse yields

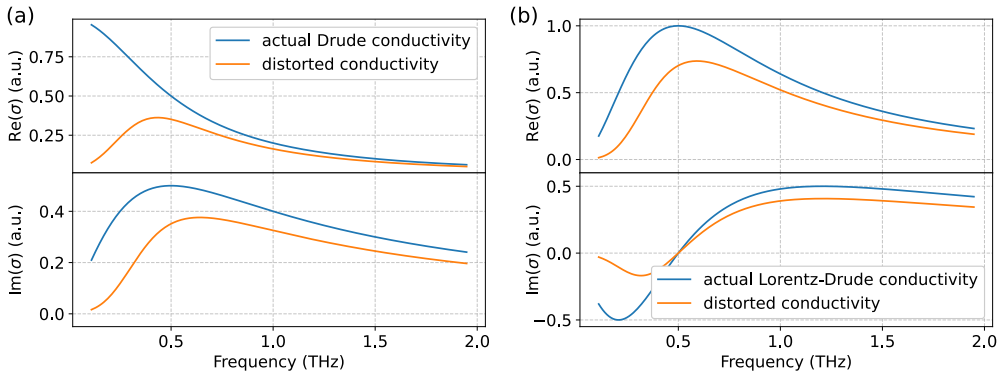

Fig. 3. Simulated perfect (a) Drude response and (b) Lorentz-Drude response and its distortion when a pump beam radius of 1.16 mm is employed and the THz beam is focused as in our setup.

approximately the frequency averaged imaginary photoconductivity [13, 14]. To assess the pump beam spot size influence on such quantities that do not require a Fourier-transformation to the frequency space, we used CdS nanowires as benchmark material and measured pump-probe scans at the THz delay of the maximum of the undisturbed THz pulse. Fig. 4(a) shows that after normalization, the frequency averaged real photoconductivity of CdS nanowires after excitation with $\lambda = 400$ nm, decays independent of the pump beam spot size. Preconditioned sufficient contrast, the frequency averaged quantities can be considered robust. However, we observe that for the largest pump beam radius of 3.02 mm, where the experiment was conducted in a non-collinear fashion, the rise time of the signal is 2.3 ps, when it is only 1.2 ps for the pump beam radius of 1.16 mm with a collinear experimental setup. Excitation at an angle results in a relative delay between opposite transverse sides of the beam such that one side of the sample is excited earlier than the other, effectively lowering the experiments temporal resolution. Thus, in such non-collinear geometry it is important to keep the angle of incidence minimum to not degrade the temporal resolution when using large pump beams. Pulse front tilting can be used to mitigate this issue and improve the temporal resolution in non-collinear setups. In this application case, the collinear arrangement is beneficial. Another approach to reduce errors is using beam-splitters to unite the beam path of pump and probe beam for collinear excitation with large pump beam spot sizes [15].

3.3.2. Charge Diffusion in highly conductive samples

In highly conductive extended samples, photoinduced charge carriers quickly diffuse after excitation. With longer delay times between optical pump and THz probe, the spatial charge carrier distribution widens, effectively changing the THz frequency range probing the photoinduced changes. The diffusivity of charge carriers in silicon after photoexcitation with a fs-laser can be as much as 1000 times higher than the room temperature diffusivity of 30 cm^2/s [16, 17]. From this, we estimate a diffusion length of 0.04 mm within 600 ps after excitation. Employing optical excitation with a beam radius of 0.54 mm on a silicon wafer, this corresponds to an expansion of the spatial charge carrier distribution of 15 %. The influence of this broadening can be demonstrated experimentally. Fig. 5(a) shows the differential THz spectrum transmitted through a Si wafer at several delay times after optical excitation with a beam radius of 0.54 mm. For frequencies larger than 1 THz, the differential THz spectrum does not change on the timescales investigated here. The pump beam spot size is large enough to homogeneously excite the part of the sample, to which the high THz frequencies are focused. However, for smaller THz frequencies,

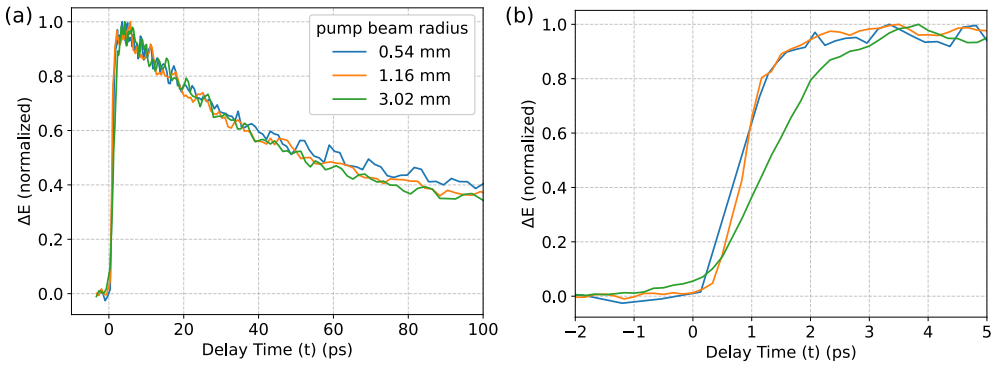

Fig. 4. (a) OPTP dynamics measured on CdS nanowires after excitation with $\lambda = 400$ nm at the maximum of the undisturbed THz pulse for different pump beam radii. No differences in the decay dynamics are observed. (b) Same data as in (a), but zoomed to shorter pump-probe delay times. For the non-collinearly pumped experiment (3.02 mm pump beam radius), the rise time is longer than for the collinearly pumped experiments (1.16 mm and 0.54 mm).

which are focused to larger spot sizes, a rise in signal is observed, as charge carriers diffuse away from the initially excited spot of the sample into the wider low-frequency probe beam spot. This leads to a time-dependent change of the transmitted spectrum in addition to the one caused by the dynamics of interest. Therefore, for investigations of high-conductivity samples, a large pump spot size, realized using a non-collinear geometry or beam-splitters, is generally required. It should be noted that charges do not only diffuse in plane but also along the excitation direction into the material, effectively thickening the excited layer, which may also lead to a change of the transmitted THz spectrum.

4. Conclusion

We discussed the distortions induced by too small pump beam spot sizes on OPTP and described them by a simple weighting of the frequency-resolved probe beam spot profiles with the spatial charge carrier distribution induced by the pump pulse. In case of frequency-dependent quantities such as the Drude model are to be discussed, a large enough pump beam spot size should be ensured. In most employed OPTP configurations, this requires a non-collinear pump-probe arrangement, which come with the downside of a reduction of temporal resolution. However, if the THz focus is characterized carefully, the distortions can also be corrected for using the overlap factor we describe. In case the OPTP dynamics are of central interest, a collinear geometry, where the optical pump pulse is overlaid with the THz probe pulse through a hole in a OAP, is beneficial. For highly conductive samples, diffusion of charge carriers away from the pump beam spot leads to larger excited areas, which yields spectral shifts in the measured differential electric field if too small pump beam spot sizes are employed.

5. Funding

This work is supported by the Cluster of Excellence ‘Advanced Imaging of Matter’ of the Deutsche Forschungsgemeinschaft (DFG) – EXC 2056 – project ID 390715994 and via the Graduate School ‘Nanohybrid‘ (GRK 2536). H.L. and F.X.K. acknowledge support within the DFG project No. 432266622.

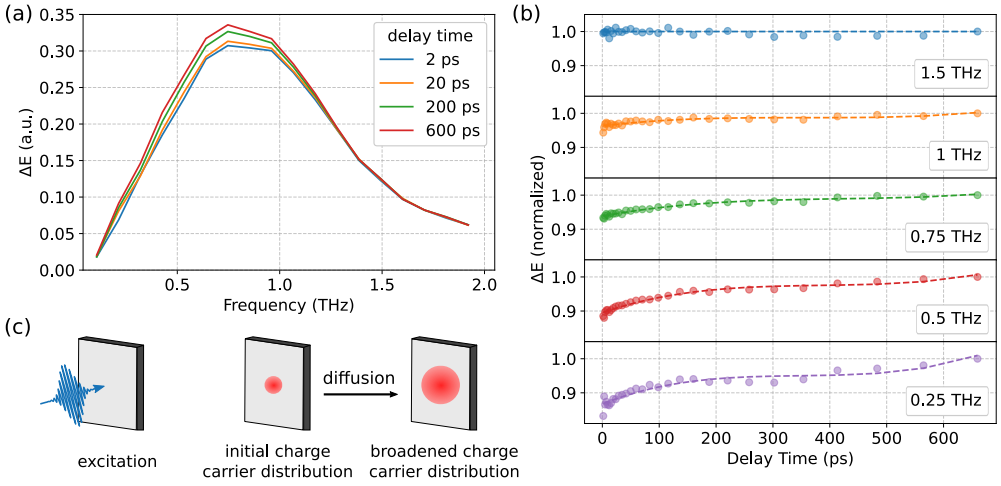

Fig. 5. (a) Measured differential THz spectrum transmitted through a Si wafer at different delay times after excitation with λ = 400 nm at an excitation fluence of 220 µJ/cm^2 with a pump beam radius of 0.54 mm. (b) Normalized differential electric fields of the measurement displayed in (a) over pump-probe delay. The initial rise in signal at short delay times is omitted for clarity. (c) Schematic representation of the observed spatial broadening in the charge carrier distribution, that leads to better overlap with low THz frequencies at later delay times.

6. Acknowledgments

The authors thank Daniel Lengle for providing the CdS nanowire sample.

7. Disclosures

The authors declare no conflicts of interest.

8. Data availability

Data underlying the results presented in this paper are not publicly available at this time but may be obtained from the authors upon reasonable request.

9. Supplemental document

See Supplement 1 for supporting content.

References

1. U. Banin, N. Waiskopf, L. Hammarström, G. Boschloo, M. Freitag, E. M. J. Johansson, J. Sá, H. Tian, M. B. Johnston, L. M. Herz, R. L. Milot, M. G. Kanatzidis, W. Ke, I. Spanopoulos, K. L. Kohlstedt, G. C. Schatz, N. Lewis, T. Meyer, A. J. Nozik, M. C. Beard, F. Armstrong, C. F. Megarity, C. A. Schmuttenmaer, V. S. Batista, and G. W. Brudvig, "Nanotechnology for catalysis and solar energy conversion," Nanotechnology **32**, 042003 (2021).
2. H. J. Joyce, J. L. Boland, C. L. Davies, S. A. Baig, and M. B. Johnston, "A review of the electrical properties of semiconductor nanowires: insights gained from terahertz conductivity spectroscopy," Semicond. Sci. Technol. **31**, 103003 (2016).
3. P. Kužel and H. Němec, "Terahertz Spectroscopy of Nanomaterials: a Close Look at Charge-Carrier Transport," Adv. Opt. Mater. **8**, 1900623 (2020).
4. Y. U. Staechelin, M. Deffner, S. Krohn, C. Castillo Delgadillo, J. S. Niehaus, and H. Lange, "Carrier localization in zero-dimensional and one-dimensional CdSe–CdS heterostructures," The J. Chem. Phys. **156**, 061102 (2022).
5. R. Ulbricht, E. Hendry, J. Shan, T. F. Heinz, and M. Bonn, "Carrier dynamics in semiconductors studied with time-resolved terahertz spectroscopy," Rev. Mod. Phys. **83**, 543–586 (2011).

6. P. Jepsen, D. Cooke, and M. Koch, "Terahertz spectroscopy and imaging - Modern techniques and applications: THz spectroscopy and imaging - Modern techniques and applications," Laser & Photonics Rev. **5**, 124–166 (2011).
7. S. L. Dexheimer, ed., *Terahertz Spectroscopy: Principles and Applications* (CRC Press, Boca Raton, 2008).
8. M. C. Beard, G. M. Turner, and C. A. Schmuttenmaer, "Transient photoconductivity in GaAs as measured by time-resolved terahertz spectroscopy," Phys. Rev. B **62**, 15764–15777 (2000).
9. G. L. Dakovski, B. Kubera, S. Lan, and J. Shan, "Finite pump-beam-size effects in optical pump-terahertz probe spectroscopy," J. Opt. Soc. Am. B **23**, 139 (2006).
10. J. H. Strait, P. A. George, M. Levendorf, M. Blood-Forsythe, F. Rana, and J. Park, "Measurements of the Carrier Dynamics and Terahertz Response of Oriented Germanium Nanowires using Optical-Pump Terahertz-Probe Spectroscopy," Nano Lett. **9**, 2967–2972 (2009).
11. L. T. Kunneman, M. Zanella, L. Manna, L. D. A. Siebbeles, and J. M. Schins, "Mobility and Spatial Distribution of Photoexcited Electrons in CdSe/CdS Nanorods," The J. Phys. Chem. C **117**, 3146–3151 (2013).
12. A. Burgos-Caminal, E. Socie, M. E. F. Bouduban, and J.-E. Moser, "Exciton and Carrier Dynamics in Two-Dimensional Perovskites," The J. Phys. Chem. Lett. **11**, 7692–7701 (2020).
13. P. D. Cunningham, "Accessing Terahertz Complex Conductivity Dynamics in the Time-Domain," IEEE Trans. on Terahertz Sci. Technol. **3**, 494–498 (2013).
14. X. Xing, L. Zhao, Z. Zhang, X. Liu, K. Zhang, Y. Yu, X. Lin, H. Y. Chen, J. Q. Chen, Z. Jin, J. Xu, and G.-h. Ma, "Role of Photoinduced Exciton in the Transient Terahertz Conductivity of Few-Layer WS $_2$ Laminate," The J. Phys. Chem. C **121**, 20451–20457 (2017).
15. L. Fekete, P. Kužel, H. Němec, F. Kadlec, A. Dejneka, J. Stuchlík, and A. Fejfar, "Ultrafast carrier dynamics in microcrystalline silicon probed by time-resolved terahertz spectroscopy," Phys. Rev. B **79**, 115306 (2009).
16. E. Najafi, V. Ivanov, A. Zewail, and M. Bernardi, "Super-diffusion of excited carriers in semiconductors," Nat. Commun. **8**, 15177 (2017).
17. R. Brunetti, C. Jacoboni, F. Nava, L. Reggiani, G. Bosman, and R. J. J. Zijlstra, "Diffusion coefficient of electrons in silicon," J. Appl. Phys. **52**, 6713–6722 (1981).